Twelfth Australasian Fluid Mechanics Conference
The University of Sydney, Australia 1995

THE EVOLUTION OF A GAS BUBBLE IN A SHALLOW WATER

Q. X. Wang, K. S. Yeo, B. C. Khoo & K. Y. Lam

Center For Computational Mechanics
and
Department of Mechanical and Production Engineering
National University of Singapore
10 Kent Ridge Crescent, Singapore 0511

ABSTRACT

The nonlinear expansion and collapse of a gas bubble in shallow water is investigated numerically. The flow is assumed to be potential and a boundary-integral method is used to solve the Laplace equation of the velocity potential. The evolution of the bubble and the free surface has been simulated and compared with those of the deep water case.

INTRODUCTION

In the last two decades, the most successful theoretical treatment of the motion of non-spherical bubble, which allows large contortion of the bubble to be followed, has been one based on numerical time integration coupled to a boundary-integral spatial solution. The method has been used to simulate the growth and collapse of bubbles near a rigid boundary by Guerri, Lucca & Prosperetti (1981), Blake, Taib & Doherty (1986), and Best & Kucera (1992). It has also been used to simulate the interaction of a bubble with a nearby free surface by Gibson & Blake (1981), Blake et al. (1987), and Wang et al. (1995). In this paper the said method is used to simulate the evolution of a bubble in shallow water where its motion is influenced by both of the sea floor and of the free water surface.

THEORETICAL ASPECTS

Consider the evolution of a gas bubble in an shallow water as shown in Fig. 1. The depth of the water is defined by h_s. The bubble is assumed to have been initiated as a tiny high-pressure spherical bubble at a distance h below the initially quiescent free surface (along z=0). The flow in the time-varying fluid domain Ω (Fig. 1) is assumed to be inviscid, incompressible and irrotational. The velocity potential $\phi(\boldsymbol{p})$ satisfies the Laplace equation and has the following integral representation:

$$c(\boldsymbol{p})\phi(\boldsymbol{p}) = \int_{\partial\Omega}\left(\frac{\partial\phi(\boldsymbol{q})}{\partial n}G(\boldsymbol{p},\boldsymbol{q}) - \phi(\boldsymbol{q})\frac{\partial G(\boldsymbol{p},\boldsymbol{q})}{\partial n}\right)dS, \quad (1)$$

where $G(\boldsymbol{p},\boldsymbol{q})$ is the Green's function due to a unit source in an infinite fluid domain plus its image about the sea bottom and

$$c(\boldsymbol{p}) = \begin{cases} 2\pi, & \boldsymbol{p} \in \partial\Omega = S \cup \Sigma_f \\ 4\pi, & \boldsymbol{p} \in \Omega. \end{cases}$$

Here $\partial\Omega$ is the boundary of the fluid domain which comprises the bubble surface S and the sea surface Σ_f. $\partial/\partial n = \boldsymbol{n}\cdot\nabla$ is the normal derivative at the boundary where $\boldsymbol{n}$ is the outward normal (see Fig. 1).

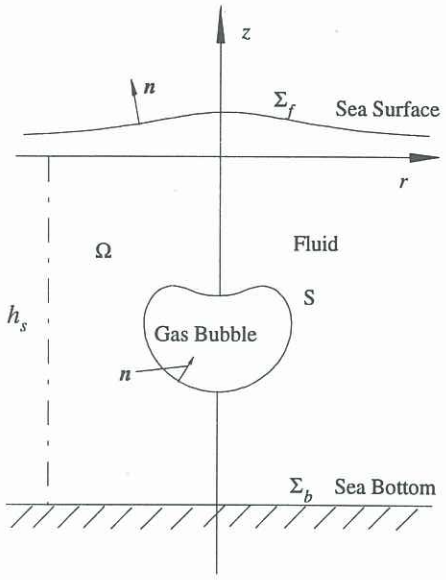

Fig. 1. Geometry and coordinate system used to model the growth and collapse of an explosion bubble in a shallow water.

The kinematic and dynamic boundary conditions governing the motion of the bubble and the free surface are

$$\frac{dx}{dt} = \nabla\phi \qquad \text{for } \boldsymbol{p} \in S \cup \Sigma_f, \quad (2\text{-}2a)$$

$$\frac{d\phi}{dt} = 1 + \frac{1}{2}|\nabla\phi|^2 + \delta^2(z-\gamma) - \varepsilon\left(\frac{V_0}{V}\right)^{\lambda} \qquad \text{for } \boldsymbol{p} \in S \quad (2\text{-}3a)$$

$$\frac{d\phi}{dt} = \frac{1}{2}|\nabla\phi|^2 + \delta^2 z \qquad \text{for } \boldsymbol{p} \in \Sigma_f. \quad (2\text{-}3b)$$

$\boldsymbol{x}$ denotes the spatial position of the particle $\boldsymbol{p}$ on $\partial\Omega$ $\varepsilon = \frac{p_0}{\Delta p}$, $\delta = (\rho g R_m/\Delta p)^{1/2}$, $\gamma = h/R_m$ are non-dimensional parameters which characterize the strength (initial pressure), the buoyancy and the initial inception position of the bubble respectively. ε and δ are termed the strength and buoyancy parameters, respectively, and $\eta = h_s/R_m$ is the non-dimensional depth of the water. Equations (1-3) form a complete set of equations which describes the evolution of the gas-filled bubble and the free surface.

The bubble is assumed to begin its existence at inception as a very tiny high-pressure spherical bubble of radius R_i with zero wall velocity. The initial radius R_i is chosen

such that its maximum radius in an infinite fluid would be equal to one.

The problem is axisymmetric along the z-axis (Fig. 1) where r is the radial coordinate. The surface of the bubble and the free surface are discretized as a set of N linear elements, each of which is locally parametrized by ξ in the range [0,1]. For the computation, the locally linear representations of the potential $\phi(\xi)$ and its derivative $\psi(\xi)$ are used. The locally linear representations of $r(\xi)$ and $z(\xi)$ are used for the calculation of influence coefficient matrix except its diagonal elements for which a cubic-spline representation of the bubble and free surface profiles has been used.

Non-uniform elements are used on the bubble and the free surface. On each surface, the lengths of the elements are arranged in an increasing ratio series. For the free surface the series begins from the axis of symmetry where the curvature is greatest; for the bubble the series begins from the expected position of the jet. After each time step, the two surfaces are interpolated by a cubic and re-discretized in the same two ratio series. For the results described in the next section, 50 elements are used on one symmetric half of the bubble and 50 elements for the free surface. The free surface elements are distributed to radial distance as large as $10R_m$.

The time integration of (2) and (3) is done by using a predictor-corrector scheme. To maintain the stability of the solution the time-step size Δt must be carefully controlled. In the present paper the time-step size Δt is chosen as

$$\Delta t = min\left\{\Delta t_1, \Delta t_2\right\}, \tag{4a}$$

$$\Delta t_1 = \frac{\Delta\phi}{max\left|1+\frac{1}{2}|\nabla\phi|^2+\delta^2(z-\gamma)-\varepsilon\left(\frac{V_0}{V}\right)^{\gamma}\right|}, \tag{4b}$$

$$\Delta t_2 = \frac{\Delta\phi}{max\left|\frac{1}{2}|\nabla\phi|^2+\delta^2 z\right|}, \tag{4c}$$

where $\Delta\phi$ is some constant. The maximum in (4b) is obtained for all the nodes defining the bubble surface, while that in (4c) is calculated for all the nodes describing the free surface. With this choice of Δt, the change in ϕ at each node is bounded above by $\Delta\phi$. The results in this work are obtained with $\Delta\phi$ kept to around 0.03.

RESULTS AND DISCUSSION

To study the shallow water effect, we simulated the following cases of $\eta=\infty$ (the infinite depth of water), 3.0, 2.0, and 1.5 while keeping ε, γ, δ constant at 100, 1.0, and 1.5, respectively. The gas bubble and free-surface profiles at selected dimensionless times t (normalized by $R_m(\rho/\Delta p)^{1/2}$) are shown in Figs. 2-5 for $\eta=\infty$, 3.0, 2.0, and 1.5, respectively.

The first case of the infinite depth of water is used for the purpose of comparison with the other cases of limited depth extent. At the end of the expansion phase (Fig. 2a), the upper part of the bubble becomes elongated. At around this moment of maximum volume, a noticeable portion of the bubble is entrained into the base of the raised free surface, hence causing a substantial free-surface hump. The Bjerknes jet is formed near the beginning of the collapse phase (Fig. 2b). The free surface in the vicinity of the axis of symmetry rises while that in the far region falls, resulting in the formation of a free surface spike.

For the case of $\eta=3.0$ (Fig. 3), the bubble is initiated at a distance of one maximum radius R_m of the bubble from the free surface and $2R_m$ from the sea bottom. The evolution of the bubble and the free surface is approximately the same as those for infinite depth of water (Fig. 2) for the whole expansion phase and most of the collapse phase. The flow field is also dominated by the Bjerknes effect of the free surface. Only at the end of the collapse phase, does the bubble move more downwards spatially and with a stronger downward jet. This can be attributed to the accentuation of the Bjerknes effect due to the presence of the rigid sea bottom.

For the case of $\eta=2.0$ (Fig. 4), the bubble is initiated at R_m both from the free surface and from the sea bottom. The effect of the shallow water becomes more noticeable towards the later stage of the expansion phase when part of the bubble surface approaches the sea bottom. During the collapse phase, the bubble is repelled by the free surface and attracted by the sea bottom due to the Bjerknes effect. In this case, the bubble migrates even more strongly downwards. A very broad and stronger Bjerknes jet is observed near the end of the collapse phase.

Finally for the case of $\eta=1.5$ (Fig. 5), the bubble is initiated at R_m from the free surface and $0.5R_m$ from the sea bottom. A large part of the bubble surface is flattened by the sea bottom in the expansion phase. The bubble is attracted by the sea bottom during the collapse phase. The Bjerknes jet is formed during the early stage of the collapse, its width is increased as the bubble collapses. At the end of the collapse phase, the bubble hugs the sea bottom with the Bjerknes jet impacting on the sea bottom as soon as it penetrates the opposite end of the bubble.

CONCLUSION

The detailed dynamical behaviour of pulsating gas products (bubble) of underwater explosions in shallow water has been successfully modelled, simulated and analyzed.

REFERENCES

Best, J. P. & Kucera, A., 1992, "A numerical investigation of non-spherical rebounding bubbles," J. of fluid Mech. 245, 137-154.

Blake, J. R. & Gibson, D. C., 1981, "Growth and collapse of a vapour cavity near free surface," *J. of Fluid Mech*, Vol. 111, pp. 124-40.

Blake, J. R., Taib, B. B. & Doherty, G. (1986) Transient cavities near boundaries. Part 1. Rigid boundary. J. Fluid Mech. 170, 479-97.

Blake, J. R., Taib, B. B. & Doherty, G., 1987, "Transient cavities near boundaries. Part 2. Free surface," *J. Fluid Mech.*, Vol. 181, pp. 197-212.

Guerri, L., Lucca, G. & Prosperetti, A. (1981) A numerical method for the dynamics of nonspherical cavitation bubbles. In Proc. 2nd Intl. Colloq. on Drops and Bubbles, 175-181. JPL publication 82-7, Monterey, California.

Wang, Q. X., Yeo, K. S., Khoo, B. C. & Lam, K. Y., "Strong interaction between buoyancy bubble and free surface," *Theoret. and Comput. Fluid Dynamics* (in press).

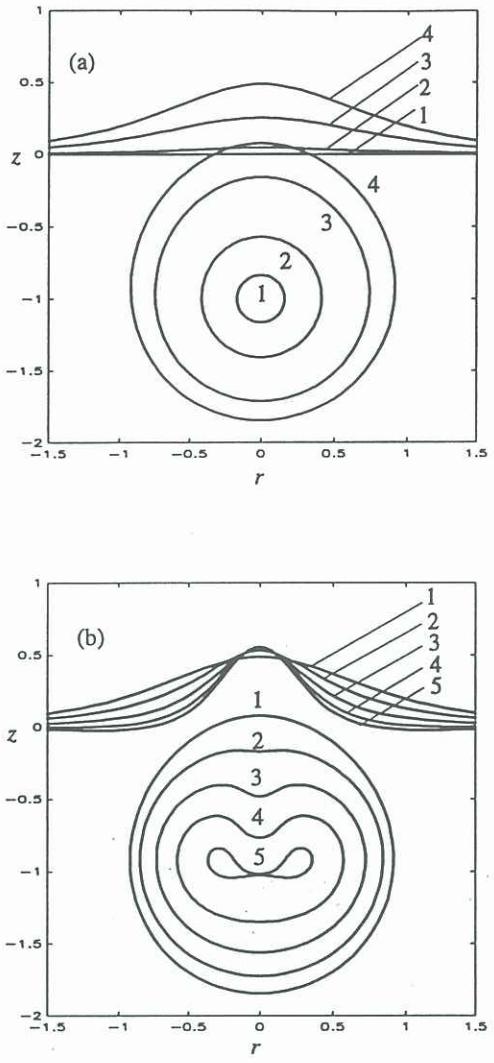

Fig. 2. Evolution of bubble and free surface shapes for $\varepsilon = 100$, $\gamma = 1.0$, $\delta = 0.5$, and $\eta = \infty$ during (a) expansion phase at dimensionless times t (1) 0.000, (2) 0.069, (3) 0. 272, (4) 0. 653, and (b) collapse phase at dimensionless times t (1) 0. 653, (2) 0947, (3) 1. 098, (4) 1.207, (5) 1. 295.

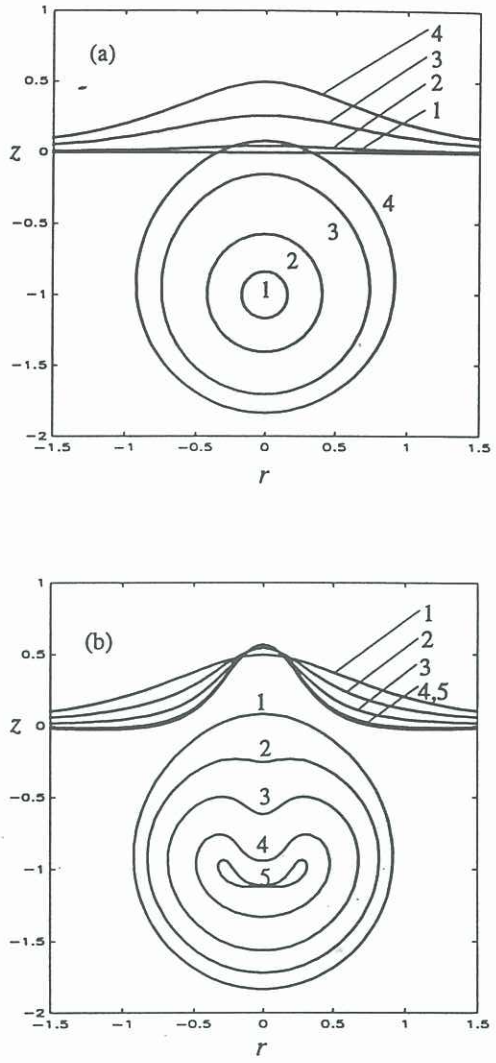

Fig. 3. Evolution of bubble and free surface shapes for $\varepsilon = 100$, $\gamma = 1.0$, $\delta = 0.5$, and $\eta = 3.0$ during (a) expansion phase at dimensionless times t (1) 0.000, (2) 0.068, (3) 0.276, (4) 0. 666, and (b) collapse phase at dimensionless times t (1) 0. 666, (2) 1.000, (3) 1. 156, (4) 1.274, (5) 1. 331.

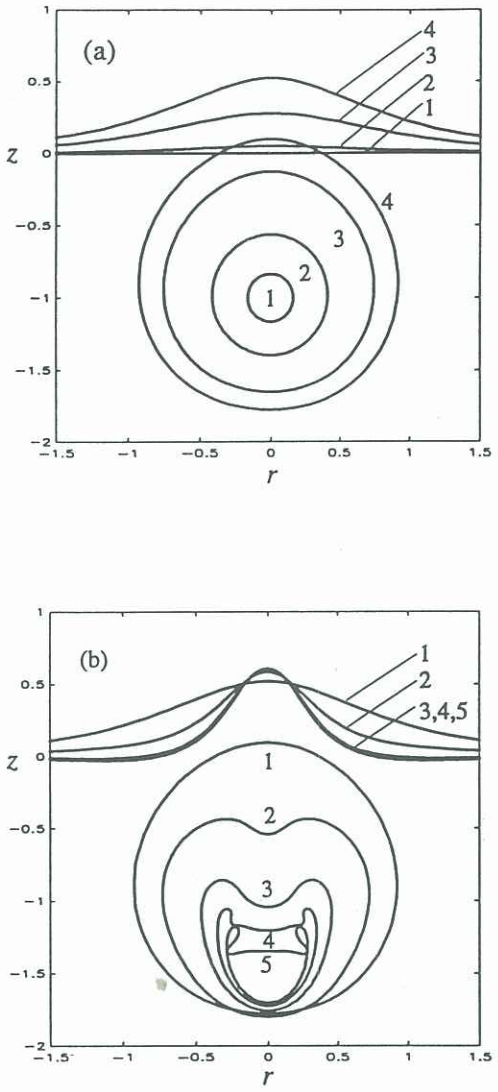

Fig. 4. Evolution of bubble and free surface shapes for $\varepsilon = 100$, $\gamma = 1.0$, $\delta = 0.5$, and $\eta = 2.0$ during (a) expansion phase at dimensionless times t (1) 0.000, (2) 0.071, (3) 0.288, (4) 0. 691, and (b) collapse phase at dimensionless times t (1) 0. 691, (2) 1.140, (3) 1. 320, (4) 1.369, (5) 1. 399.

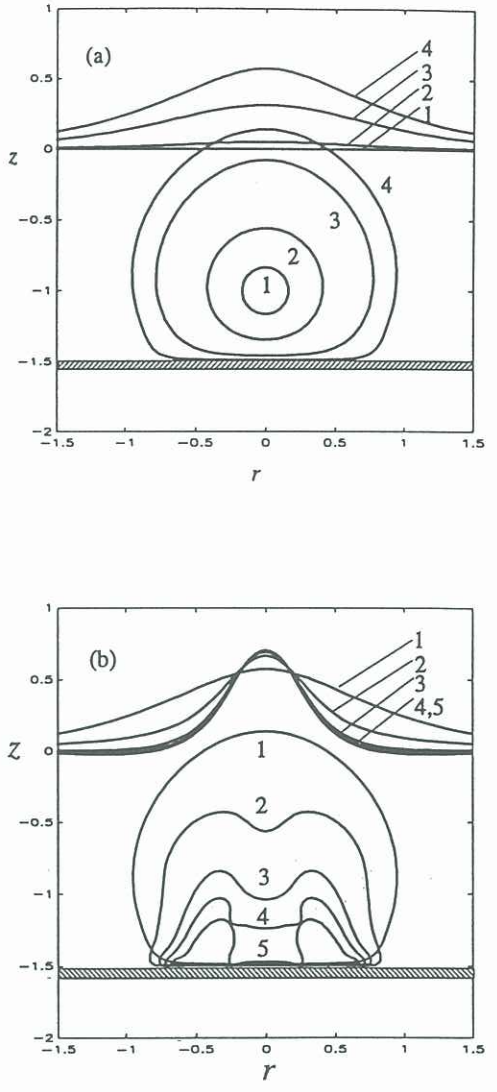

Fig. 5. Evolution of bubble and free surface shapes for $\varepsilon = 100$, $\gamma = 1.0$, $\delta = 0.5$, and $\eta = 1.5$ during (a) expansion phase at dimensionless times t (1) 0.000, (2) 0.071, (3) 0. 307, (4) 0. 719, and (b) collapse phase at dimensionless times t (1) 0. 719, (2) 1. 174, (3) 1. 342, (4) 1. 401, (5) 1. 454.